POLITECNICO DI TORINO
Repository ISTITUZIONALE

Solvent-Driven Supramolecular Wrapping of Self-Assembled Structures

Original
Solvent-Driven Supramolecular Wrapping of Self-Assembled Structures / Moreno-Alcantar, G., Aliprandi, A., Rouquette, R., Pesce, L., Wurst, K., Perego, C., Bruggeller, P., Pavan, G.M., De Cola, L.. - In: ANGEWANDTE CHEMIE. INTERNATIONAL EDITION. - ISSN 1433-7851. - 60:10(2021), pp. 5407-5413. [10.1002/anie.202013474]

Availability:
This version is available at: 11583/2883975 since: 2021-04-06T13:01:49Z

Publisher:
Wiley-VCH Verlag

Published
DOI:10.1002/anie.202013474

Terms of use:

This article is made available under terms and conditions as specified in the corresponding bibliographic description in the repository

Publisher copyright

(Article begins on next page)

08 September 2026

Check for updates

Supramolecular Chemistry

How to cite: *Angew. Chem. Int. Ed.* **2021**, *60*, 5407–5413
International Edition: doi.org/10.1002/anie.202013474
German Edition: doi.org/10.1002/ange.202013474

Solvent-Driven Supramolecular Wrapping of Self-Assembled Structures

Guillermo Moreno-Alcántar, Alessandro Aliprandi, Remi Rouquette, Luca Pesce, Klaus Wurst, Claudio Perego, Peter Brüggeller, Giovanni M. Pavan,* and Luisa De Cola**

Abstract: *Self-assembly relies on the ability of smaller and discrete entities to spontaneously arrange into more organized systems by means of the structure-encoded information. Herein, we show that the design of the media can play a role even more important than the chemical design. The media not only determines the self-assembly pathway at a single-component level, but in a very narrow solvent composition, a supramolecular homo-aggregate can be non-covalently wrapped by a second component that possesses a different crystal lattice. Such a process has been followed in real time by confocal microscopy thanks to the different emission colors of the aggregates formed by two isolated Pt^{II} complexes. This coating is reversible and controlled by the media composition. Single-crystal X-ray diffraction and molecular simulations based on coarse-grained (CG) models allowed the understanding of the properties displayed by the different aggregates. Such findings could result in a new method to construct hierarchical supramolecular structures.*

Introduction

Over the past decade, a rapid evolution in the field of supramolecular polymerization has led to a greater control over the size and architecture of supramolecular assemblies.[1–6] Kinetic experiments have further increased the complexity of such fascinating process by revealing the presence of off-pathway aggregates that can buffer the free monomer and prevent unwanted nucleation process.[7] Such discoveries have driven the development of novel strategies to enhance the control of the supramolecular polymerization. For example by designing monomers able to establish intramolecular hydrogen bonds that stabilize the monomeric species,[8,9] or by blocking the monomers into metastable aggregates avoiding unwanted nucleation.[10] Supramolecular structures with controlled length and narrow polydispersity have been obtained by converting metastable aggregates into the thermodynamic assembly by seeded growth in a fashion that reminds a biological infection process.[10,11] Our group has reported a system where a luminescent amphiphilic Pt^{II} complex can be kinetically trapped into metastable micelles and then transformed into thermodynamically stable nanoribbons.[12] In our case, the key point was to study the effect of the solvent composition on self-assembly process taking advantage of the dynamic change of the photoluminescent properties of these Pt^{II} complexes.[12–14] Indeed, in square planar platinum compounds, containing conjugated flat ligands, aggregation can occur, and novel molecular orbital can arise from Pt-Pt interactions.[15] In particular the formation of such electronic interactions leads to different photophysical properties of the monomer vs. the aggregated species, due to the interaction of dz^2 orbitals in the Pt centers.[16–19] Such dynamic behavior has resulted in the unprecedented real-time visualization of the self-assembly process. In the quest for supramolecular co-aggregates based on this kind of compounds, it has been reported the use of block polymers that can, in turn, interact electrostatically with different components.[20,21]

So far, all the attempts to co-assembly or hierarchically organize different units has been relying either on different ligands that could interact to form intermolecular bonds[22,23] or identical ligands with different metals possessing the same geometry,[24–26] or chromophores.[5] Indeed, the control of co-

[*] Dr. G. Moreno-Alcántar, Dr. A. Aliprandi, Dr. R. Rouquette, Prof. L. De Cola
Institut de Science et d'Ingénierie Supramoléculaires (ISIS)
Université de Strasbourg & CNRS
8 allée Gaspard Monge, 67083 Strasbourg (France)
E-mail: aliprandi@unisttra.fr
decola@unistra.fr

Dr. L. Pesce, Dr. C. Perego, Prof. G. M. Pavan
Department of Innovative Technologies, University of Applied Sciences and Arts of Southern Switzerland
Galleria 2, via Cantonale 2c, 6928 Manno (Switzerland)

Dr. K. Wurst, Prof. P. Brüggeller
Center for Chemistry and Biomedicine, University of Innsbruck
Innrain 80–82, 6020 Innsbruck (Austria)

Prof. G. M. Pavan
Department of Applied Science and Technology, Politecnico di Torino
Corso Duca degli Abruzzi 24, 10129 Torino (Italy)
E-mail: giovanni.pavan@polito.it

Prof. L. De Cola
Institute for Nanotechnology (INT)
Karlsruhe Institute of Technology
Hermann-von-Helmholtz-Platz 1, 76344 Eggenstein-Leopoldshafen (Germany)

Supporting information and the ORCID identification number(s) for the author(s) of this article can be found under: https://doi.org/10.1002/anie.202013474.

© 2020 The Authors. Angewandte Chemie International Edition published by Wiley-VCH GmbH. This is an open access article under the terms of the Creative Commons Attribution Non-Commercial NoDerivs License, which permits use and distribution in any medium, provided the original work is properly cited, the use is non-commercial and no modifications or adaptations are made.

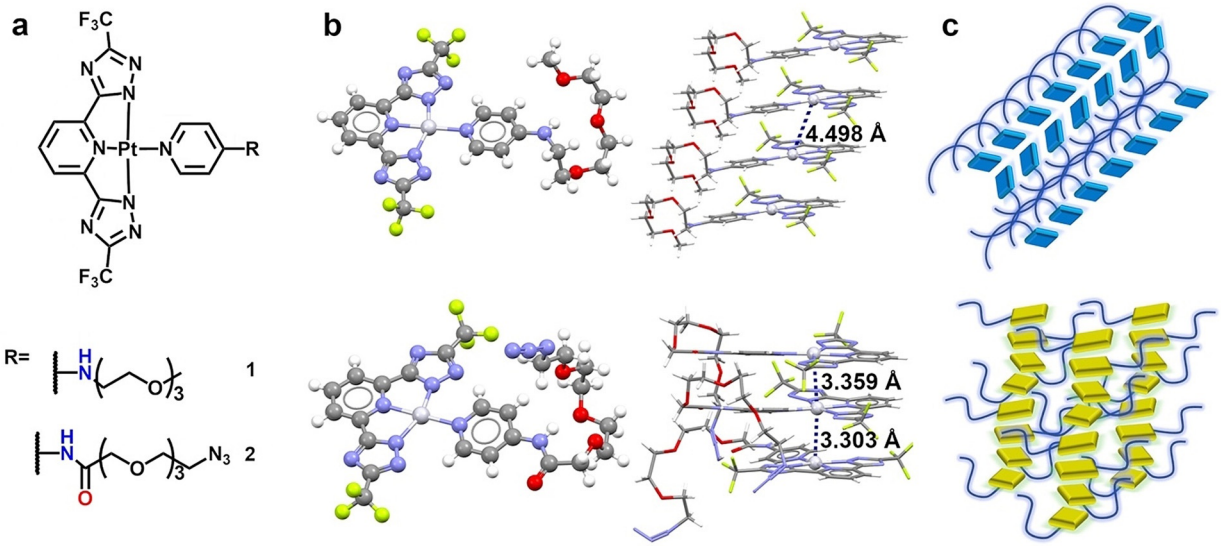

Figure 1. a) Structures of compounds **1** and **2**. b) Top: Molecular structure of **1** determined by single-crystal X-ray diffraction and aggregated structure of the compound showing the long Pt-Pt distance. Bottom: molecular structure of **2** determined by single-crystal X-ray diffraction and π-stacked structure of compound **2** showing the short Pt-Pt distances. c) Schematic representation of the packing observed in compounds **1** (top) and **2** (bottom).

assembly of metal complexes with different crystal lattice has not been reported. Such difficulties are related to the tendency to self-sorting of the two different components in solution to form large supramolecular structures. However, in a very specific media, such assembly can deviate from the expected homo-packing and co-assembly, hetero-packing, can occur.

We show that two Pt^{II} complexes **1**[12] and **2** (Figure 1a) which coordinate distinct ancillary ligands, possess dissimilar self-assembly behavior and, in the same media, the packing of the complexes is drastically different since they self-sort in solution to form blue emitting nanoribbons, complex **1**, and yellow emitting fibers, complex **2**. The thermodynamic structures of both the homo-assemblies have been determined by single crystal X-ray diffraction. However, by a fine tuning of the polarity of the media it is possible to stabilize the nanoribbons of **1** and apply on them a molecular wrapping by **2** leading to a supramolecular co-assembly. The reversibility of the coating has been unambiguously proved by real-time confocal imaging and spectroscopic techniques. As questioned by Whitesides and Grzybowsky "Is anything not self-assembly?"[27] We think that everything could be assembled or even co-assembled if the chemical structure and the media are both carefully designed.

Results and Discussion

Co-Assembly Components

The crystal structure of the blue emitting form of compound **1** is shown in Figure 1b, the asymmetric unit is composed of a single molecule. It could be observed that the ethylene glycol chain is bended by the intramolecular hydrogen bonds between the oxygens and the amino group. Besides the intramolecular interactions the ring formation is stabilized by numerous intermolecular hydrogen bonds of glycol chains of different molecules (Figure S9). Such packing causes a displacement of the Pt units that are not aligned and the resulting distance, along the *b* crystallographic axis is 4.4984(8) Å. This distance is considerably longer than the sum of van der Waals radii of platinum (3.32).[28,29] As a consequence electronic interactions at distances above 3.5 Å do not take place, and this explains the lack of MMLCT transitions[12] and the blue emissive nature of the compound.

In **2**, the longer oligoethylene glycol chain introduce more disorder and the nearly linear conformation precludes the formation of the intramolecular interactions observed for **1**. As a consequence a stronger electronic coupling between the Pt units is observed, induced by the short distance between two adjacent metal ions (< 3.5 Å) (Figure 1c). In detail, the asymmetric unit in the crystal is formed by three molecules, two of them displaying disorder in the ethyleneglycol chains with 60/40 and 50/50 occupancy factors. This inefficient packing does not promote lamellar hydrogen bonded domains like those observed in **1** (Figure S10). Therefore, the metallophilic stacked synthon drives in **2** the formation of the aggregates. The shorter Pt-Pt distances (3.3585(6), 3.3256(6) and 3.3030(6) Å) in this compound are consistent with the MMLCT transitions, resulting, upon light excitation, in the characteristic yellow emission of the aggregates formed by the compound **2**.

Self-Assembly of Compound 2

Compound **2** has shown to have a strong tendency to form aggregates in solution. NMR studies have revealed an important enthalpy of self-aggregation of $\Delta H_{agg} = -31.3\ KJ\,mol^{-1}$ in 1,4-dioxane (details are given in SI).[30] In order to study how the media controls the self-assembly

 © 2020 The Authors. Angewandte Chemie International Edition published by Wiley-VCH GmbH

behavior of **2** we have performed depolymerization studies monitoring the luminescent properties as a function of the solvent composition with an integrating sphere setup as already reported for compound **1**.[12] After the flash injection of 250 μL of 1×10^{-3} M dioxane solution of **2** in 4.750 mL of water (the resulting concentration is 5×10^{-5} M) the compound associates in aggregates (**2A**) of hydrodynamic diameter of c.a. 321 nm, Figure S20, (for **1a** the dynamic diameter is 126 nm[12]) and PLQY of 90% with an emission maximum at 590 nm (Figure S1). Then aliquots of molecularly dissolved **2** in pure dioxane ($c=5\times10^{-5}$ M) were added to change the solvent composition while keeping the overall concentration of the complex constant. The resulting depolymerization curve (Figure 2a) shows the formation of a second self-assembled species (**2B**) with a ≈20 nm blue-shifted emission (Figure 2b) and a PLQY close to 20% at water content above 65%. Further decrease of the water ratio results in a complete dissolution of the structures and a drop of the PLQY <1%. Kinetic experiments carried out at 65:35 water:dioxane ratio by confocal fluorescence microscopy have shown that a time zero no large aggregates are observed since addition of the dioxane caused the evolution of the yellow-orange aggregates in the fibers that are visible after 30 minutes. The emission properties of the yellow-green fibers (assembly **2B**) has an energy and features that corresponds to the final assemblies that can grow over time, see Figure 2e and Supplementary Movie 1. The broadness and energy of the emission spectrum of the fibers indicates the existence of Pt-Pt metallophilic interactions, which we expect less pronounced than at higher water concentration because of the blue shift of the emission maxima from 590 nm to 570 nm upon change in the solvent composition. SEM images show that assembly **2B** have ribbon-like morphology with sharp shape and width of 1.0–2.0 μm (Figure S18).

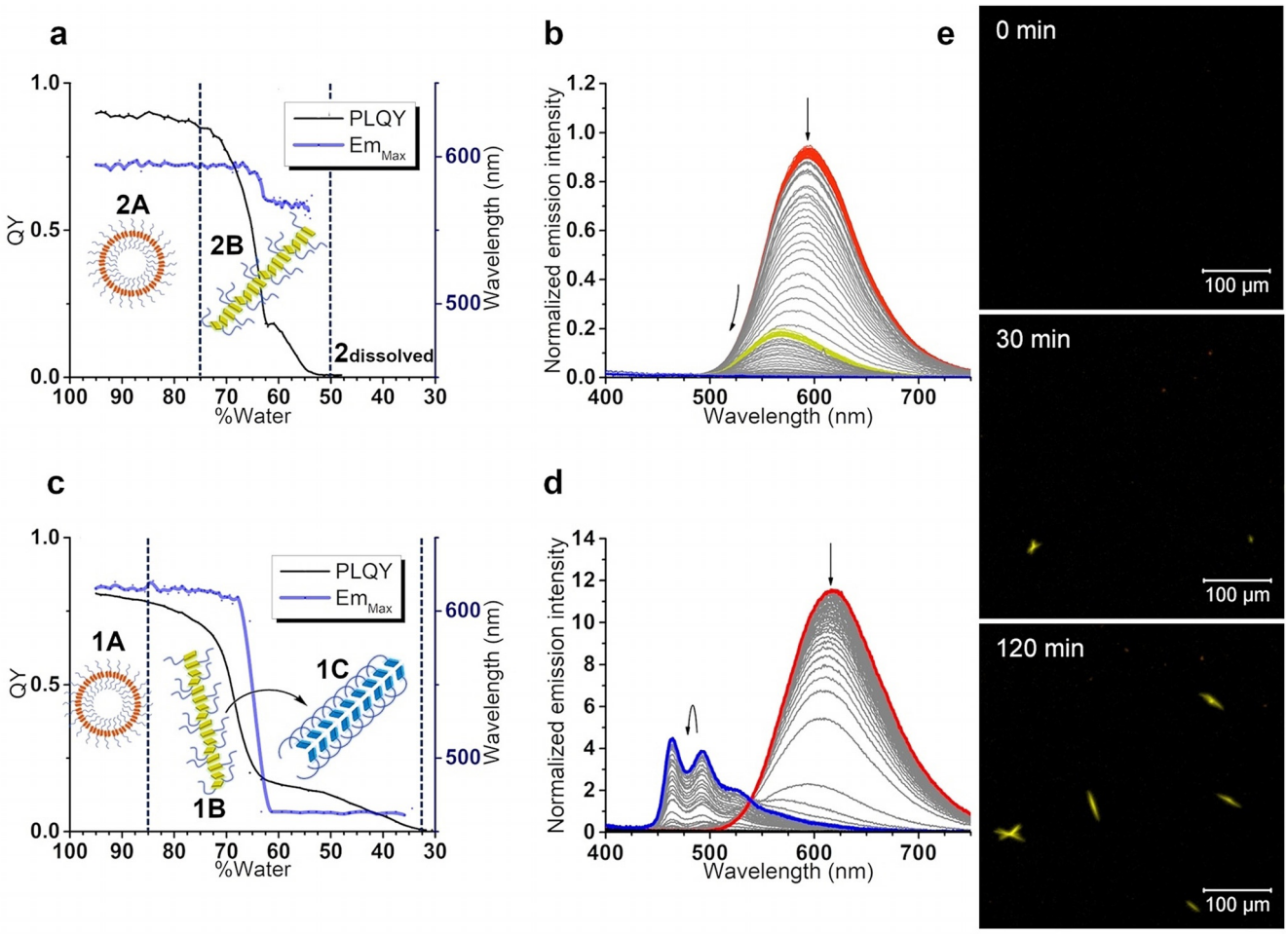

Figure 2. a) Depolymerization profile of compound **2** ($c=5\times10^{-5}$ M) showing the PLQY and emission maximum, as a function of the ratio water:dioxane in the system. b) Spectra profile of the depolymerization experiment for **2**, from the starting orange emissive aggregates at high water content (red line spectra) to a second class of yellow-emissive structures (yellow line) below 70% water content, to the molecularly dissolved state when the water content is below 50% (blue line), $\lambda_{ex}=313$ nm. c) Depolymerization profile of compound **1** ($c=1\times10^{-4}$ M) showing the PLQY and emission maximum, as a function of the % of water in the system. d) Spectra profile of the depolymerization experiment for **1**, the starting orange-emissive aggregates at high water content (red line spectra) to a the blue-emitting nanoribbons (blue line) below 70% water content to the molecularly dissolved state when the water content is below 30%, $\lambda_{ex}=313$ nm. Spectra profile of the depolymerization experiment for **1** adapted, with permission of Springer Nature, from ref. [12]. e) Snapshots taken from Supplementary Movie 1 showing the time-dependent evolution of the yellow assemblies (**2B**) by confocal microscopy at 65% water content ($\lambda_{ex}=405$ nm) (more information is provided in the SI).

 © 2020 The Authors. Angewandte Chemie International Edition published by Wiley-VCH GmbH

This behavior of **2** differs from that previously observed in compound **1**, in which the self-assembly pathway consists of two kinetically trapped species: micellar orange emitting aggregates (**1A**) and yellow emitting fibers (**1B**), which are in equilibria with the dissolved form of the compound. These aggregates finally evolve to the thermodynamically stable blue emitting ribbons (**1C**) as shown by its depolymerization profile (Figure 2c,d). In contrast, in **2** the yellow fibers **2B** are not a kinetically trapped state but the thermodynamically stable form. Consequently, once those fibers are formed, they do not evolve into different aggregates. Making a parallel analysis of these two landscapes we propose that the **B** forms of both **1** and **2** are structurally similar, but in the case of **1** the competition with other supramolecular interactions in the self-assembly process, that is, hydrogen-bonding, drives to the formation of **1C** aggregates while for **2** the stability of the final assembly is dominated by the Pt-Pt interactions. This hypothesis is supported by the previously discussed single-crystal X-ray diffraction structures of **1C** blue and **2B** yellow.

Co-Assembly

Since the thermodynamically favored supramolecular assemblies of **1** and **2** can be easily distinguished in terms of emission colors, we investigated the possibility to obtain co-assemblies of these complexes. In particular, we hypothesized that such a goal can be reached by a fine tuning of the solvent composition. As it can be observed from the depolymerization curves (Figure 2a,c) the dissolution of the blue fibers (assembly **1C**) requires a higher amount of 1,4-dioxane compared to the one required to dissolve the yellow fibers **2B**. We expected that between 50 and 65% water content the nucleation of complex **2** would be rather inhibited allowing **1C** to act as seed. Therefore, a sample containing **1A** ($C_1 = 5 \times 10^{-5}$ M) in 60% water was allowed to evolve towards the formation of the supramolecular blue aggregates **1C** and then (after 6 hours) mixed (1:1) with a freshly prepared solution containing **2A** at the same concentration and solvent composition. The mixture was set in a closed quartz Petri dish and observed in real time by confocal microscopy (Figure 3a, Supplementary Movie 2).

Interestingly a lag time of around 30 minutes has been observed after which the blue fibers start to be covered by a yellow emitting layer of **2B**. After 160 min, almost a complete wrapping of the fibers was observed. Surprisingly once they are fully coated no further growth is observed.

If complex **2** is not added to the solution, no change in the blue fibers is observed even after several days, indicating that the yellow emission is indeed originated by the self-assembly of complex **2** on the surface of the nanoribbons **1C**. SEM images of the coated fibers (Figure S19) show a change in the structure, particularly noticeable in the tips, in comparison with the pristine nanoribbons of **1C**.[12] Due to the easier dissolution of **2B** respect to **1C**, as revealed by the depolymerization curves (Figure 2a,c), we expect to be able to remove the self-assembled coating restoring assembly **1C** by changing the solvent composition. Thus, the dioxane content on the system was increased slowly by diffusing dioxane vapors inside a quartz petri dish while monitoring the system by confocal microscopy (supplementary Movie 3 and Figure 3b). Indeed, the dissolution of the **2B** structures reveals the presence of a blue-emitting ribbon structure underneath which has templated the wrapping of **2** and upon dissolution the assembled **1C** structure maintain the initial shape, size and emission color.

Since in our experimental condition complex **2** in 60% water is already aggregated in **2A**, we do not know if the interaction between the blue fibers of **1** and complex **2** is leading to the dissolution of **2A**, in monomeric units, or the assembly itself can aggregate on top of **1**. As revealed by the depolymerization profile (Figure 2a), when the water content is 50% or less, **2** exists as molecularly dissolved species. Therefore to clarify the behavior described above we studied the interactions of **1C** (Figure 2c)[12] and **2** in the molecularly dissolved form. Similarly to what is stated above, a change in the color of the fibers without a noticeable change in shape or size was observed. The **1C** structures were molecularly coated and a yellow emission is observed due to the assembly of **2** (Supplementary Movie 4 and Figure S13). Further de-coating test shows the process is equally reversible (Figure S14).

This wrapping phenomenon has been observed only in the range of water content between 50 and 60%. Already at 65% water content formation of **2B** homo-fibers is observed along with the co-assembly process (Figure S15). At higher water content the self-sorted assembly is favored and only homo-fibers are observed while the coating does not occur. Therefore, the only experimental condition to allow the co-assembly is a narrow choice of the ratio between water and dioxane. In any other solvent composition, either the common self-sorting occurs or the supramolecular structures are soluble and the hetero-assembly is not a competitive path in solution. The fact that the coating pathway opens when the non-aqueous character of the media increases might be an indicative of the mode of association of compound **2** to defects originated on the surface of compound **1** fibers. This increase in the polarity may disturb the packing in the surface, letting π-stacking sites exposed at the surface to which compound **2** could attach seeding the formation of the coating layer.

To investigate this hypothesis we use molecular simulations based on coarse-grained (CG) models[31–33] of monomers **1** and **2** with the MARTINI force-field[34] (Figure 4a). In Figures 4b and 4c, we report the self-assembled structures for the **1** and **2** cases obtained after 2.5 μs of CG-MD at 60% water content. Consistently with the experimental evidence, we observe the formation of fibrillar aggregates in both systems, and presence of core-core stacking between the monomers. Such monomer stacks interact further via hydrophobic interactions, forming larger elongated assemblies. We note that system **1** forms one single supramolecular fiber that percolates through the boundaries of the periodic simulation box, while the assembly of **2** appears as less directional and ordered. To assess the uniformity of the assembled fiber of **1**, we calculated the interaction energy of the individual monomers with the rest of the fiber ($\Delta E_1(i)$) and determined how strongly, or weakly, each monomer is incorporated into the

 © 2020 The Authors. Angewandte Chemie International Edition published by Wiley-VCH GmbH

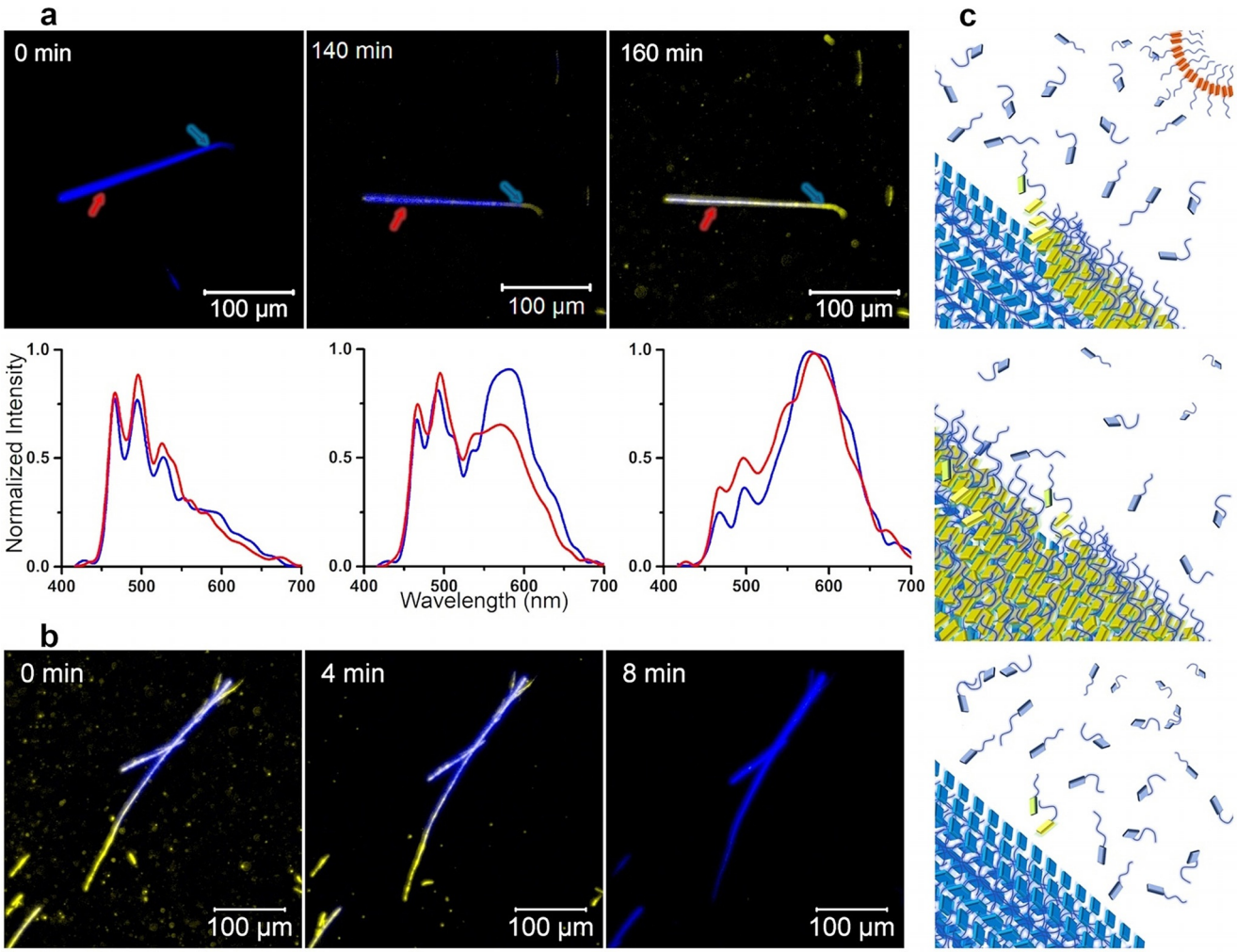

Figure 3. a) Top: Confocal microscopy time-progression of the evolution of the wrapping by compound **2** on the preformed fibers of compound **1** at 60% water content (Snapshots taken from Supplementary Movie 2). Bottom: Emission spectra (recorded under the microscope) in different parts of the fiber (arrows indicate the point of acquisition) corresponding to the times shown in the top pictures (λ_{ex} = 405 nm). b) Snapshots taken from Supplementary Movie 3 showing the confocal microscopy time-progression of the disassembly of **2** from fibers **1C** (λ_{ex} = 405 nm). c) Schematic representation of: (top) the coating process by **2** on fibers **1C** as depicted in panels a), (medium) the scenario after the coating process and (bottom) the representation after the de-coating experiment promoted by the change in solvent composition (panels b).

assembly compared to the average monomer interaction energy ($<\Delta E_1>$). $\Delta E_1(i)/<\Delta E_1>$ values smaller/greater than 1 identify monomers that are more weakly/strongly incorporated in fiber **1**. We also calculated the Solvent Accessible Surface Area (SASA) of each monomer in the assembly ($SASA_1(i)$), which determines its degree of exposition to the solvent and compared to the average in the fiber **1** (as $SASA_1(i)/<SASA_1>$). Plotting these parameters we identify defects in fiber **1**, as those monomers which are more exposed to the solvent and weaker incorporated in the assembly than the average (Figure 4d, red dots). These defects are key for the dynamics and monomer exchange in these fibers.[32] Such defects represent possible spots from which monomers **2** can enter fiber **1**, and thus pathways for 1–2 copolymerization and interactions.[35,36]

To explore the co-assembly of **2** onto a pre-formed fiber of **1** monomers, we then simulated a self-assembled fiber **1** immersed in a solution (water:1,4-dioxane = 60%:40%) containing dissolved **2** monomers. We performed CG-MD simulations where fiber **1** (composed of 400 assembled **1** monomers) is surrounded by a different number of **2** monomers (i.e., 50, 100 and 200). The results of these simulations in Figure 4e demonstrate that the **2** monomers tend to form small aggregates, or stacks (in yellow), which bind and nucleate onto the defects present on the surface of fiber **1** (in red). The plot in Figure 4e shows that, in presence of **2** monomers, the **1** monomers in the assembly reduce significantly their SASA and simultaneously increase their interaction with the rest of the fiber **1**. This is due to the binding of **2** with the most exposed monomers of fiber **1** (red monomers Figure 4d), the effect becomes more and more relevant as the number of **2** monomers in the system increased. This provides a molecular-level picture in agreement with the coating phenomenon detected by experiments. These results also support the crucial role of structural defects in regulating the co-assembly, consistently with what recently evidenced in the study of other supramolecular systems.[32,37]

 © 2020 The Authors. Angewandte Chemie International Edition published by Wiley-VCH GmbH

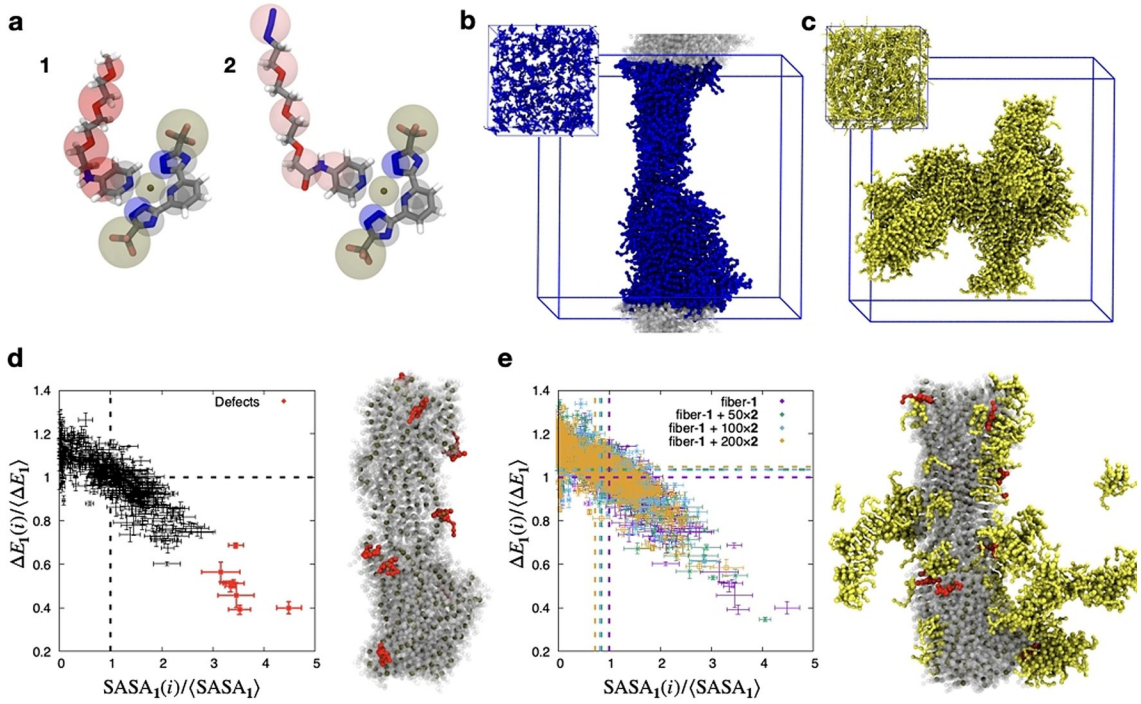

Figure 4. a) Molecular models of monomers **1** and **2**: all-atom (solid stick) and CG (superimposed transparent spheres) monomer models. b) Snapshots of the self-assembly of **1** monomers (in blue) into fiber **1** (solvent not shown for clarity) after 2.5 μs of CG-MD. The inset shows the initial configuration with dispersed monomers. c) Same as panel b, for the self-assembly of **2** monomers (in yellow). d) Identification of defects in fiber **1**: plot of the interaction energy $\Delta E_1(i)$ of the individual **1** monomers with all the other monomers in fiber **1** as a function of their SASA (and $\langle SASA_1\rangle$ are the average values over all monomers, indicated by dashed black lines in the plot). Defects are displayed as red points. e) Copolymerization with **2** proceeds through defects: plot of the $\Delta E_1(i)$ and SASA of the individual **1** monomers for increasing amounts of **2** monomers in the system. Different colors correspond to a different amount of **2** monomers in solution. The dashed lines indicate the average values for each series of data (**1** monomers become less and less exposed to the solvent and more strongly interacting with the rest of fiber **1** when surrounded by **2** monomers). The co-assembly data are extracted after 2.5 μs of CG-MD. The snapshot shows the co-assembly of 200 **2** monomers (yellow) with fiber 1 (grey, defects highlighted in red) after 2.5 μs of CG-MD.

Conclusion

Altogether, the X-ray determined structures have provided insights into the self-assembly motifs of this kind of platinum complexes revealing the structural factors driving the self-recognition pathways revalorizing the important effects of the modification of distant ancillary groups. In particular, we presented, in real time, a supramolecular coating process of a self-assembled structure by a different compound. Besides, our experiments show how this process is reversible and that it involves the direct interaction of the dissolved species with the supramolecular self-assembled entities. All the self-assembly and co-assembly processes are controlled by the composition of the media and the latest occurs only in a very narrow range when the water amount is between 50 and 65 % revealing that the environment in which the self-assembly takes place plays an even more important role than the chemical design.

Acknowledgements

G.M.-A. acknowledges the support of CONACYT-Mexico Postdoctoral grant number 740732. P. Brüggeller thanks the EFRE within the project SolarHydrogen for financial support. It is funded by resources of the state of Tyrol together with the European Union. G.M.P. acknowledges the funding received by the Swiss National Science Foundation (SNSF grants IZLIZ2_183336 and 200021_175735) and by the European Research Council (ERC) under the European Union's Horizon 2020 research and innovation program (grant agreement n°. 818776—DYNAPOL). L.D.C. thanks IUF and Axa for financial support. The authors also acknowledge the computational resources provided by the Swiss National Supercomputing Center (CSCS) and by CINECA. Open access funding enabled and organized by Projekt DEAL.

Conflict of interest

The authors declare no conflict of interest.

Keywords: luminescence · metal–metal interactions · platinum · self-assembly · supramolecular chemistry

[1] D. van der Zwaag, T. F. A. de Greef, E. W. Meijer, *Angew. Chem. Int. Ed.* **2015**, *54*, 8334 – 8336; *Angew. Chem.* **2015**, *127*, 8452 – 8454.
[2] X. Wang, G. Guerin, H. Wang, Y. Wang, I. Manners, M. A. Winnik, *Science* **2007**, *317*, 644 – 647.

 © 2020 The Authors. Angewandte Chemie International Edition published by Wiley-VCH GmbH

[3] J. B. Gilroy, T. Gädt, G. R. Whittell, L. Chabanne, J. M. Mitchels, R. M. Richardson, M. A. Winnik, I. Manners, *Nat. Chem.* **2010**, *2*, 566 – 570.
[4] M. E. Robinson, D. J. Lunn, A. Nazemi, G. R. Whittell, L. De Cola, I. Manners, *Chem. Commun.* **2015**, *51*, 15921 – 15924.
[5] Z. M. Hudson, D. J. Lunn, M. A. Winnik, I. Manners, *Nat. Commun.* **2014**, *5*, 3372.
[6] Z. Yu, F. Tantakitti, T. Yu, L. C. Palmer, G. C. Schatz, S. I. Stupp, *Science* **2016**, *351*, 497 – 502.
[7] M. Wehner, F. Würthner, *Nat. Rev. Chem.* **2020**, *4*, 38 – 53.
[8] S. Ogi, V. Stepanenko, K. Sugiyasu, M. Takeuchi, F. Würthner, *J. Am. Chem. Soc.* **2015**, *137*, 3300 – 3307.
[9] J. Kang, D. Miyajima, T. Mori, Y. Inoue, Y. Itoh, T. Aida, *Science* **2015**, *347*, 646 – 651.
[10] S. Ogi, K. Sugiyasu, S. Manna, S. Samitsu, M. Takeuchi, *Nat. Chem.* **2014**, *6*, 188 – 195.
[11] E. T. Powers, D. L. Powersy, *Biophys. J.* **2008**, *94*, 379 – 391.
[12] A. Aliprandi, M. Mauro, L. De Cola, *Nat. Chem.* **2016**, *8*, 10 – 15.
[13] S. Sinn, F. Biedermann, L. De Cola, *Chem. Eur. J.* **2017**, *23*, 1965 – 1971.
[14] M. Mauro, A. Aliprandi, C. Cebrián, D. Wang, C. Kübel, L. De Cola, *Chem. Commun.* **2014**, *50*, 7269 – 7272.
[15] V. W.-W. Yam, V. K.-M. Au, S. Y.-L. Leung, *Chem. Rev.* **2015**, *115*, 7589 – 7728.
[16] M. H.-Y. Chan, M. Ng, S. Y.-L. Leung, W. H. Lam, V. W.-W. Yam, *J. Am. Chem. Soc.* **2017**, *139*, 8639 – 8645.
[17] M. Ward, *Platinum Met. Rev.* **2009**, *53*, 45 – 47.
[18] Z. Chen, A. Lohr, C. R. Saha-Möller, F. Würthner, *Chem. Soc. Rev.* **2009**, *38*, 564 – 584.
[19] Y. Han, Z. Gao, C. Wang, R. Zhong, F. Wang, *Coord. Chem. Rev.* **2020**, *414*, 213300.
[20] K. Zhang, M. C.-L. Yeung, S. Y.-L. Leung, V. W.-W. Yam, *Proc. Natl. Acad. Sci. USA* **2017**, *114*, 11844 – 11849.
[21] K. Zhang, M. C. L. Yeung, S. Y. L. Leung, V. W. W. Yam, *Chem* **2017**, *2*, 825 – 839.
[22] Z. Li, Y. Han, F. Wang, *Nat. Commun.* **2019**, *10*, 3735.
[23] V. C.-H. Wong, C. Po, S. Y.-L. Leung, A. K.-W. Chan, S. Yang, B. Zhu, X. Cui, V. W.-W. Yam, *J. Am. Chem. Soc.* **2018**, *140*, 657 – 666.
[24] J. P. Coelho, J. Matern, R. Q. Albuquerque, G. Fernández, *Chem. Eur. J.* **2019**, *25*, 8960 – 8964.
[25] Q. Wan, W.-P. To, X. Chang, C.-M. Che, *Chem* **2020**, *6*, 945 – 967.
[26] G. Marinescu, S. Ferlay, N. Kyritsakas, M. Wais Hosseini, *Chem. Commun.* **2013**, *49*, 11209 – 11211.
[27] G. M. Whitesides, *Science* **2002**, *295*, 2418 – 2421.
[28] A. Bondi, *J. Phys. Chem.* **1964**, *68*, 441 – 451.
[29] S. Alvarez, *Dalton Trans.* **2013**, *42*, 8617.
[30] "supramolecular.org," can be found under supramolecular.org, **2020**.
[31] A. Sarkar, R. Sasmal, C. Empereur-mot, D. Bochicchio, S. V. K. Kompella, K. Sharma, S. Dhiman, B. Sundaram, S. S. Agasti, G. M. Pavan, et al., *J. Am. Chem. Soc.* **2020**, *142*, 7606 – 7617.
[32] D. Bochicchio, M. Salvalaglio, G. M. Pavan, *Nat. Commun.* **2017**, *8*, 147.
[33] D. Bochicchio, G. M. Pavan, *Adv. Phys. X* **2018**, *3*, 1436408.
[34] S. J. Marrink, H. J. Risselada, S. Yefimov, D. P. Tieleman, A. H. de Vries, *J. Phys. Chem. B* **2007**, *111*, 7812 – 7824.
[35] P. Gasparotto, D. Bochicchio, M. Ceriotti, G. M. Pavan, *J. Phys. Chem. B* **2020**, *124*, 589 – 599.
[36] R. P. M. Lafleur, S. M. C. Schoenmakers, P. Madhikar, D. Bochicchio, B. Baumeier, A. R. A. Palmans, G. M. Pavan, E. W. Meijer, *Macromolecules* **2019**, *52*, 3049 – 3055.
[37] D. Bochicchio, S. Kwangmettatam, T. Kudernac, G. M. Pavan, *ACS Nano* **2019**, *13*, 4322 – 4334.

Manuscript received: October 6, 2020
Revised manuscript received: November 18, 2020
Accepted manuscript online: November 27, 2020
Version of record online: January 21, 2021

 © 2020 The Authors. Angewandte Chemie International Edition published by Wiley-VCH GmbH